HHS Public Access

Author manuscript

Exp Eye Res. Author manuscript; available in PMC 2020 April 01.

Published in final edited form as:

Exp Eye Res. 2019 April ; 181: 49–60. doi:10.1016/j.exer.2019.01.017.

Impact of topical anti-fibrotics on corneal nerve regeneration *in vivo*

Holly B. Hindman[1,2], **Margaret DeMagistris**[1], **Christine Callan**[1], **Thurma McDaniel**[1], **Tracy Bubel**[2], and **Krystel R. Huxlin**[1,2]

[1]The Flaum Eye Institute, University of Rochester, Rochester, NY 14642, USA.

[2]Center for Visual Science, University of Rochester, Rochester, NY 14627, USA.

Abstract

Recent work *in vitro* has shown that fibroblasts and myofibroblasts have opposing effects on neurite outgrowth by peripheral sensory neurons. Here, we tested a prediction from this work that dampening the fibrotic response in the early phases of corneal wound healing *in vivo* could enhance reinnervation after a large, deep corneal injury such as that induced by photorefractive keratectomy (PRK). Since topical steroids and Mitomycin C (MMC) are often used clinically for mitigating corneal inflammation and scarring after PRK, they were ideal to test this prediction. Twenty adult cats underwent bilateral, myopic PRK over a 6mm optical zone followed by either: (1) intraoperative MMC (*n=12* eyes), (2) intraoperative prednisolone acetate (PA) followed by twice daily topical application for 14 days (*n=12* eyes), or (3) no post-operative treatment (*n=16* eyes). Anti-fibrotic effects of MMC and PA were verified optically and histologically. First, optical coherence tomography (OCT) performed pre-operatively and 2, 4 and 12 weeks post-PRK was used to assess changes in corneal backscatter reflectivity. Post-mortem immunohistochemistry was then performed at 2, 4 and 12 weeks post-PRK, using antibodies against α-smooth muscle actin (α-SMA). Finally, immunohistochemistry with antibodies against βIII-tubulin (Tuj-1) was performed in the same corneas to quantify changes in nerve distribution relative to unoperated, control cat corneas. Two weeks after PRK, untreated corneas exhibited the greatest amount of staining for α-SMA, followed by PA-treated and MMC-treated eyes. This was matched by higher OCT-based stromal reflectivity values in untreated, than PA- and MMC-treated eyes. PA treatment appeared to slow epithelial healing and although normal epithelial thickness was restored by 12 weeks-post-PRK, intra-epithelial nerve length only reached ~1/6 normal values in PA-treated eyes. Even peripheral cornea (outside the ablation zone) exhibited depressed intra-epithelial nerve densities after PA treatment. Stromal nerves were abundant under the α-SMA zone, but appeared to largely avoid it, creating an area of sub-epithelial stroma devoid of nerve trunks. In turn, this may have led to the lack of sub-basal and intra-epithelial nerves in the ablation zone of PA-treated eyes 4 weeks after PRK, and their continuing paucity 12 weeks after PRK. Intra-operative MMC,

Correspondence and reprint requests: Dr. Krystel R. Huxlin, PhD, Flaum Eye Institute, Box 659; University of Rochester Medical Center; 210 Crittenden Blvd, Rochester, NY 14642, USA; phone +1-585-275-5495; khuxlin@ur.rochester.edu.

There are no conflicts of interest for any of the authors.

which sharply decreased α-SMA staining, was followed by rapid restoration of nerve densities in all corneal layers post-PRK compared to untreated corneas. Curiously, stromal nerves appeared unaffected by the development of large, stromal, acellular zones in MMC-treated corneas. Overall, it appears that post-PRK treatments that were most effective at reducing α-SMA-positive cells in the early postoperative period benefited nerve regeneration the most, resulting in more rapid restoration of nerve densities in all corneal layers of the ablation zone and of the corneal periphery.

Keywords

prednisolone acetate; epithelium; sub-basal layer; stroma; laser refractive surgery; wound healing

1. INTRODUCTION

In addition to its transparency and critical role in focusing light onto the retina, the cornea is the most sensitive and densely innervated tissue in the human body (Shaheen et al., 2014). Corneal nerves are mostly nociceptive and mechanosensitive, coding discomfort and pain in response to mechanical, heat/cold and chemical stimulation; they also control the blink reflex, tear production and tear secretion (reviewed in Belmonte et al., 2004a; Marfurt et al., 2010b; Müller et al., 2003; Shaheen et al., 2014), all of which are involved in protecting the eye, maintaining corneal health and optimizing vision. In human and non-human primates, as well as [relevant to the present study] in cats, corneal nerves arise from the ophthalmic division of the trigeminal ganglion; in contrast with the innervation of rabbit and rodent corneas (comparative anatomy reviewed in Chan-Ling, 1989), axons of trigeminal neurons enter the cat and human corneas at the limbus but separate into two domains. The peripheral cornea is innervated by branches of conjunctival nerves that enter at the sub-epithelial and stromal levels, and then quickly ramify into basal epithelial leashes and intraepithelial nerves. The central cornea's innervation derives from thick nerve cords that travel from the periphery to the center through the deeper stroma, and which ramify anteriorly to form the sub-basal plexus, from which derive the central, intra-epithelial nerves (Chan-Ling, 1989; Guthoff et al., 2005; Marfurt et al., 2010a; Muller et al., 2003). These similarities in corneal nerve origins and anatomy between cats and humans (Chan-Ling, 1989) make felines a particularly good animal model in which to study nerve regeneration following corneal injury in humans.

Corneal disease, infection and surgery can all damage corneal nerves, with long-term consequences that range from blindness (Yamada et al., 2008) to pain (Belmonte et al., 1997; Murata and Masuko, 2006) and dry eye (Labbe et al., 2013). Yet our knowledge of factors controlling corneal nerve regeneration after damage in the large, human cornea remains relatively poor. As a result, in recent times, there has been a proliferation of research, especially using mouse animal models of corneal injury and nerve regeneration (e.g. Bech et al., 2018; Harris et al., 2018; Ozaki et al., 2018; Stepp et al., 2018; Zhang et al., 2018). Several of these studies have shown an interplay between immune cells and corneal nerves (e.g. Sarkar et al., 2013; Seyed-Razavi et al., 2014)), as well as between nerves and the corneal epithelium, including stem cells (Araki et al., 1994; Beuerman and Schimmelpfennig, 1980; Goins, 2005; Ueno et al., 2012). In laboratory work, a common

approach to enhance corneal nerve regeneration is to enhance epithelial regeneration and apply growth factors such as nerve growth factor or vascular endothelial growth factor to the surface of the eye (Guaiquil et al., 2014; Lambiase et al., 2012). More recently, attention has also turned to the interaction between nerves and stromal keratocytes, fibroblasts, or myofibroblasts (Jeon et al., 2018; Yam et al., 2017). Keratocytes occupy and synthesize the bulk of the cornea's volume (the stroma), and are critical for maintaining the cornea's unique optical and structural properties; however, they also transform into fibroblasts and scar-forming, alpha-smooth muscle actin (α-SMA)-positive myofibroblasts during wound healing (Bühren et al., 2009; Huxlin et al., 2013; Jester et al., 2003; Jester et al., 1999; Nagy et al., 2007; Wilson, 2002; Wilson et al., 2001). As recently reported by Jeon and colleagues *in vitro* (Jeon et al., 2018), feline myofibroblasts inhibit neurite extension in co-cultured sensory neurons. The present set of experiments were designed to assess a prediction based on these *in vitro* results: that inhibiting myofibroblast differentiation early during corneal wound healing *in vivo*, should enhance reinnervation of the wound area. To do this, we contrasted nerve densities in feline corneas for a period of 3 months after PRK followed by either intra-operative MMC, topical steroids or no treatment. PRK induces a similarly strong, reproducible fibrosis and myofibroblast differentiation in humans (Esquenazi et al., 2005; Netto et al., 2005) and cats (Bühren et al., 2009; Bühren et al., 2007a; Bühren et al., 2007b; Huxlin et al., 2013; Jeon et al., 2014; Nagy et al., 2007). It is also a procedure in which topical steroids and MMC have been shown to decrease post-operative inflammation and fibrosis (Majmudar et al., 2000; Vigo et al., 2003). Experimentally, PRK was ideal to achieve our goals because it damages nerves in all three corneal layers they populate: the epithelium, sub-basal layer and stroma. Cats were chosen as the preferred animal model for this investigation because their large, thick corneas bear strong structural and biological similarities to the human cornea (Bahn et al., 1982; Hughes, 1977; Jester et al., 1992). In particular, the large feline cornea allowed us to perform human-sized PRK over a 6mm optical zone, with an 8mm transition zone. Moreover, the cat cornea permitted the study of nerve regeneration in the context of a wound healing reaction that took weeks to months to unravel, providing a better match for the temporal and cellular dynamics of wound healing that can occur in the large, human cornea (Bahn et al., 1982; Jester et al., 1992).

Following PRK, we estimated the strength of fibrosis attained in the different treatment groups by measuring backscatter reflectivity *in vivo* using corneal optical coherence tomography (OCT), and post-mortem immunostaining for alpha smooth muscle actin (α-SMA), an indicator of myofibroblast differentiation (Netto et al., 2006a). Staining for beta III-tubulin (Tuj-1) of the same tissue sections was used to quantify nerve distributions in all corneal layers, providing the most complete yet perspective on nerve regeneration post-PRK.

Anti-inflammatory steroids such as prednisolone acetate (Carones et al., 1993; Fagerholm et al., 1994; Gartry et al., 1993; Machat, 1993) and intra-operative MMC (Gambato et al., 2005; Kim et al., 2004; Majmudar et al., 2000; Netto et al., 2006b; Santhiago et al., 2012; Schipper et al., 1997) are commonly used to manipulate wound healing and mitigate fibrosis after laser vision correction surgery in humans. Curiously though, whereas corticosteroids are known to function as anti-fibrotics in other tissues such as lung, breast and kidney (Miller et al., 2006; Moreira et al., 2010; Shoji et al., 2000), whether they inhibit myofibroblast differentiation in the cornea has not been determined. What has been shown is

their ability to suppress production of inflammatory chemokines in *already-activated* corneal myofibroblasts (Ebihara et al., 2011). Theoretically, this should reduce the strength of the fibrotic reaction following PRK. MMC after PRK has been used for many years by refractive surgeons, specifically to block haze (reviewed in Majmudar et al., 2000; Salomao and Wison, 2009). In addition to killing a range of cells in the anterior stroma, MMC is thought to be an effective anti-fibrotic because it also inhibits mitosis of - among others - progenitor subtypes that would normally differentiate into myofibroblasts and populate the anterior stroma (Kim et al., 2004; Netto et al., 2006b). All in all, based on their effects in humans, both topical steroids and MMC are expected to decrease fibrosis post-PRK in the cat, although relative efficacy, time-course and mechanisms of action would differ. This in turn, offers a unique opportunity to assess whether and to what degree the strength and duration of myofibroblast differentiation after injury impact reinnervation of the central cornea.

2. METHODS

Experiments were performed on 44 eyes from normal, healthy, adult, domestic, short-hair cats (*felis cattus*). All cats were obtained from a research breeding colony managed by Liberty Research Inc. (Waverley, NY, USA). Tissues and cat used in the present study came from animals either vaccinated with a killed vaccine that covers feline panleukopenia, rhinotracheitis (herpes virus) and calici (Fel-O-Vax PCT + Calicivax), or from animals confirmed sero-negative for Herpes Simplex Virus serotype I (HSV-1) and maintained in isolation. This included 4 eyes that served as unoperated controls, and 40 eyes from 20 cats that underwent bilateral PRK (Table 1). All cats were fed a research grade, quality Purina food that was nutritionally complete and balanced, for the entire duration of the study. Animal procedures were conducted according to the ARVO statement for the Use of Animals in Ophthalmic and Vision Research, and the NIH Guide for the Care and Use of Laboratory Animals. The protocol was approved by the University of Rochester Committee on Animal Research (Assurance Number: A-3292–01).

2.1. Photorefractive keratectomy (PRK)

Cats were placed under topical (0.5% proparacaine, Falcon, Fort Worth, TX) and surgical anesthesia (5mg/kg ketamine, 0.04 mg/kg dexmedetomidine hydrochloride). After epithelial debridement over a central area ~10mm in diameter, a −10 diopter (D) spherical ablation (Planoscan 4.35A, Bausch and Lomb Inc.) was performed in the stromal bed with a Technolas 217 laser (Bausch and Lomb Inc.), generating a central ablation depth of ~135 μm over a 6 mm optical zone (OZ) plus a 1.55 mm transition zone (Planoscan 4.35A) manually centered over the pupil. As reported in our previous, published work in the cat, likely due to a combination of different biomechanics, corneal dimensions and laser ablation rates in cats *versus* humans, a −10D intended ablation over 6 mm OZ in cats results in about a third of the intended refractive correction (e.g., Bühren et al., 2009; Nagy et al., 2007). As such, the −10D feline PRK was optimal for the intended goals of the present study, approximating a human equivalent that would be closer to a −3D or −4D ablation.

2.2. Pharmacological treatments post-PRK

Eyes were randomly assigned to one of three groups, receiving either no treatment, 1% prednisolone acetate (PA, Pacific Pharma, Irvine, CA), or 0.02% MMC (Mobius Therapeutics, LLC, St Louis, MO). MMC was applied intra-operatively and held in place on the ablated stromal bed using a saturated, sterile, gelatin sponge (Surgifoam™; Ethicon) for 1 minute immediately post-PRK, followed by copious irrigation. PA was also applied to the stromal bed immediately after PRK, but it was then re-applied as a topical eye drop twice daily for 14 days post-PRK. All cats also received a drop of antibiotic solution topically to the eye (Neomycin, Polymyxin B Sulphate, Gramicidin Ophthalmic Solution USP, Bausch & Lomb Inc.) twice daily for 2 weeks post-PRK.

2.3. Histology and immunohistochemistry

In addition to the unoperated eyes, a proportion of the cats were euthanized for histology 2, 4 and 12 weeks post-PRK (Table 1). They received an overdose of sodium pentobarbital (Sleepaway, Fort Dodge Animal Health, Fort Dodge, Iowa). Corneas were excised and immersion-fixed in 1% paraformaldehyde in 0.1M phosphate buffered saline (PBS), pH 7.4 for 10 minutes. They were then transferred to 30% sucrose in 0.1M PBS, and stored at 4°C for 2 days. The tissue was embedded in Tissue Tek O.C.T. Compound (Sakura Finetek) and frozen, serial, 20μm-thick, transverse sections were cut using a cryostat (2800 Frigocut E, Reichert-Jung), collected on gelatin-coated slides and stored at −20°C until stained. For PRK-treated eyes, 1 in every 20 slides was first stained with Hematoxylin and Eosin (H&E) using standard protocols to identify the ablation zone, which was roughly in the center of affected corneal sections. For all but the MMC-treated eyes, the ablation zone was defined by a cellular hyper-density in the stroma immediately underlying the epithelium. MMC-treated eyes lacked such a hyper-density in the stroma, but instead, exhibited a marked, localized thickening of the epithelial layers over a markedly thinned ablation zone.

Slides close to the ablation center were then selected for immunohistochemistry and nerve density analysis. In unoperated corneas, slides were selected from the center of each cornea. Corneal sections were first treated with a blocking step, which consisted of a 30 mins incubation in a solution made of 5% normal horse serum (NHS) in 0.1M phosphate buffered saline (PBS) with 0.1% Triton X-100 prior to the application of primary antibodies, which were also diluted in this blocking solution. After rinsing, sections were incubated with primary antibodies overnight at 4°C. These included a rabbit polyclonal anti- alpha-smooth muscle actin (α-SMA, staining myofibroblasts; ab5694 Abcam, Cambridge, MA; 1:400) antibody and a mouse monoclonal anti-beta III-tubulin antibody (Tuj-1, staining corneal nerves; MMS-435P, Covance, Princeton, NJ; 1:1000). Some sections from each treatment group were also incubated overnight with only PBS containing 5% NHS and 0.1% Triton X-100 as a negative control. After rinsing, secondary antibodies were applied: Alexa Fluor 488 conjugated to goat anti-rabbit IgG (A11008, Invitrogen, Grand Island NY; 1:400) and Alexa Fluor 555 conjugated to goat anti-mouse IgG (A21422, Invitrogen, Grand Island, NY; 1:400). After incubation at room temperature for two hours, sections were rinsed and cover-slipped with DAPI (4′,6-diamidino-2-phenylindol)-Vectashield Mounting Medium (Vector Laboratories, Burlingame, California).

2.4. Fluorescence imaging, tracing and analysis of corneal nerve distribution

Our goal in the present study was to evaluate the impact of PRK and different anti-fibrotic treatments on corneal nerve regeneration during the early post-operative period in the cat. To do this, we contrasted the distribution of corneal nerves in the epithelium and stroma of corneal cross-sections that were triple-labeled with markers fluorescing blue (DAPI-labeled cell nuclei), green (α-SMA) and red (Tuj-1-positive nerves).

Four to six immuno-stained sections were analyzed per eye at each time-point for each treatment group, as well as for unoperated, control eyes. Sections were considered suitable for analysis if they possessed histologically-intact epithelium and stroma, as well as immuno-labeling for all markers of interest (cell nuclei, Tuj1, and αSMA, where present). Stained sections were first imaged using an Olympus BX53 microscope equipped with a motorized stage and interfaced either through a Q Imaging camera (Quantitative Imaging Corporation, Surrey, BC, Canada) or with an ORCA-Flash 4.0 LT Digital CMOS camera (Hamamatsu Photonics K.K., Japan) with a computer running a Neurolucida software workstation (MicroBrightField Biosciences, Williston, VT). Pictures of the selected corneal sections (for examples, see Fig. 1A) were first collected using a 10x objective and the appropriate fluorescent cubes (Semrock, Rochester,NY). The captured images were then traced manually in Neurolucida, first outlining the entire corneal section with a closed contour. The process was repeated to generate a contour around the epithelium, as well as around any α-SMA-positive or acellular zones (if present). Each Tuj-1-positive nerve fiber was then traced, and color-coded to indicate those segments that passed through the corneal stroma, the epithelium, and zones of the stroma that were either α-SMA positive or acellular (see Fig. 1B for labeling scheme in an intact, control cornea). This allowed Neurolucida to compute several measurements for each whole corneal section traced: the total corneal area, the area occupied by the epithelium, α-SMA positive staining and the area of acellular zones. Within each of these areas, we also summed the total length of nerves. For illustrative purposes, the traces were exported out of Neurolucida using Neurolucida Explorer (MicroBrightField Biosciences, Williston, VT) and saved as TIFF files. In parallel, the quantitative data was exported out of Neurolucida into an Excel spreadsheet for further analysis.

Quantitative analysis was performed over a box 2390μm × 1350μm placed in the approximate center of the ablation zone and in the mid-periphery (half-way between the outer edge of the ablation zone and the edge of the cornea) of each drawn section. In all cases, the drawn section was first rotated in Neurolucida until it was aligned to the auto-move box and the magnification was reduced to 4x. The box was drawn over the region of interest (ablation center or periphery); the corneal sub-regions contained within the box (epithelium, stroma, regions of α-SMA staining and acellular zones) were outlined manually and their areas were measured. The length of nerves in each of the sub-regions inside a given box were automatically computed and exported using Neurolucida Explorer (MicroBrightField Biosciences, Williston VT) into an Excel spreadsheet, where we computed the total nerve length in the sub-basal layer, and a nerve density index (NDI) for the epithelium and stroma. The NDI was calculated by dividing total nerve length within the

epithelium (L_e) or stroma (L_s) by the area of the epithelium (A_e)or stroma (A_s) within the box:

$$NDI_e = L_e/A_e$$

$$NDI_s = L_s/A_s$$

All values were then averaged across at least 2–3 sections/eye, for all eyes in each group and time-point.

2.5. Optical Coherence Tomography (OCT)

A custom-built, 1310 nm anterior segment OCT (Nagy et al., 2007; Radhakrishnan et al., 2001; Wang et al., 2004) was used to quantify corneal backscatter light intensity from images collected under anesthesia (5mg/kg ketamine, 0.04 mg/kg dexmedetomidine hydrochloride) at 2, 4 and 12 weeks post-PRK. A video stream of the central cornea was captured at 8Hz, and 10 images were extracted from each video for analysis. A profile of pixel intensities was generated as previously reported (Nagy et al., 2007; Radhakrishnan et al., 2001; Wang et al., 2004). Using ImageJ (NIH), we quantified pixel intensity along 4 lines drawn perpendicular to the corneal surface (Fig. 2A), as previously described (Bühren et al., 2009; Bühren et al., 2007b; Bühren et al., 2010; Huxlin et al., 2013; Jeon et al., 2014; Nagy et al., 2007). The first two lines were positioned ~100μm on either side of the corneal center to avoid the area of specular reflectivity. The other lines were placed 50μm peripheral to the first lines. The pixel intensity profile from epithelium to endothelium was averaged across all 4 lines and normalized to the mean pixel intensity in a background region external to the cornea, to compensate for fluctuations in laser strength (Fig. 2B). The region corresponding to the stroma was then divided into thirds (Fig. 2B) to compute the mean, normalized pixel intensity over the anterior and posterior thirds of the cornea for each image. This was then averaged across 10 images for each eye and time-point.

2.6. Statistical Analyses

When three or more intervention groups were compared, inter-group differences were compared with one or two-way analyses of variance (ANOVAs), followed by Tukey's post-hoc tests, as appropriate. When only two groups were compared, two-tailed paired or unpaired Student's t-tests were performed. A probability of error of $P<0.05$ was considered statistically significant.

3. RESULTS

3.1. Corneal nerve distribution in intact, adult cat eyes

Similar to human corneas, the normal cat cornea possesses a regular epithelium 7–9 layers thick, with a basal layer of cuboidal cells aligned against a basement membrane (Fig. 1A). Below the epithelium lies a collagenous stroma ~550μm thick. The anterior third or so of the stroma is populated by chords of Tuj-1 positive nerve fibers (red traces in Fig. 1B), while the

posterior half is entirely devoid of nerves. Between the stroma and epithelium lay the sub-basal nerve plexus from which fine Tuj-1 positive branches emerge, penetrating the epithelium almost perpendicularly (Fig. 1A; orange traces in Fig. 1B). These intra-epithelial nerves span the epithelial thickness, ending close to the ocular surface. They are densest centrally (mean ± SEM central NDI_e = 16 ± 1.4 mm/mm^2), and sparsest in the peripheral cornea (mean peripheral NDI_e = 7.9 ± 0.8 mm/mm^2). In contrast, central and peripheral NDI_s were similar, at 0.5 ± 0.04 mm/mm^2 and 0.4 ± 0.05 mm/mm^2 respectively. Sub-basal nerve length also remained relatively constant between central and peripheral cornea, averaging 0.9 ± 0.1 mm and 0.7 ± 0.1 mm, respectively.

3.2. Fibrosis post-PRK in the cat: effect of MMC and PA

OCT imaging and histology showed MMC and PA to exert anti-fibrotic effects in cats after PRK. Preoperatively, the normalized OCT reflectivity of the anterior stroma (mean ± SEM, untreated: 1.59±0.06, PA: 1.64±0.06, and MMC: 1.64±0.06) and posterior stroma (untreated: 1.41±0.05, PA: 1.38±0.05, MMC: 1.42±0.06) were similar between treatment groups (Figs. 3A, B). Two weeks after PRK, stromal reflectivity in the anterior 1/3 of the cornea was significantly higher than baseline in all treatment groups (repeated measures ANOVA: $F(1,39)=137.5, p<0.0001$), but the increase was larger in untreated corneas than in corneas treated with anti-fibrotics (one-way ANOVA: $F(2, 39)=4.88, p=0.0128$; post-hoc Tukey HSD tests: untreated *versus* MMC $p<0.05$, untreated *versus* PA $p<0.05$, MMC *versus* PA not significant; Fig. 3B). Stromal reflectivity of the posterior 1/3 of the stroma also increased post-PRK (repeated measures ANOVA: $F(1,39)=63, p<0.0001$), but the change was smaller in magnitude than that in the anterior stroma and was similar across treatment groups (one-way ANOVA: $F(2, 39)=0.41, p=0.67$, Fig. 3B).

Immunohistochemically, the α-SMA band 2 weeks post-PRK appeared thickest in untreated eyes (Fig. 3C), thinning at 4 weeks (Fig. 3D) and disappearing by 12 weeks post-PRK (Fig. 3E). PA-treated eyes had moderate α-SMA at 2 weeks (Fig. 3F) but seemed to experience a rebound or at least maintenance in α-SMA positivity once topical treatment stopped; as such, the α-SMA positive bands appeared qualitatively the same or larger 4 weeks post-PRK (Fig. 3G) than at 2 weeks post-PRK, disappearing by 12 weeks post-PRK (Fig. 3H). MMC-treated eyes had a very thin α-SMA band at 2 weeks post-PRK, with significant α-SMA-free gaps in the sub-epithelial stroma (Fig. 3I). By 4 weeks post-PRK, MMC-treated corneas were completely devoid of α-SMA staining (Fig. 3J), remaining so out to 12 weeks post-PRK (Fig. 3K).

3.3. Corneal nerve distribution after PRK in the cat

Debridement and PRK destroyed all nerves in the epithelium and sub-basal layer of a central zone ~7.5 mm in diameter, as well as stromal nerves in that same region, to a depth of about 135μm. In the absence of post-operative treatment with either steroids or MMC, we made the following observations:

3.3.1. Two weeks after PRK,—Both OCT (Fig. 3A) and histology (Fig. 3C) showed that a thin epithelium had regenerated across the entire, debrided stromal bed. Centrally, this epithelium measured about half its normal thickness (baseline = 54±2.5 μm). As mentioned

above, a strong, thick, αSMA-positive band (green in Figs. 3C, top row in Fig. 4) occupied the stroma just under the healed epithelium. As previously reported (Jeon et al., 2018), although this region of stroma should have contained nerves (see central NDIs reported above for unoperated cats), the αSMA-positive band was almost completely devoid of them, with an $NDI_{\alpha SMA}$ of 0.01 ± 0.002 mm/mm^2 (Fig. 3C, top row Fig. 4). This was all the more surprising as the central stroma below the αSMA-positive zone contained >3x the normal density of Tuj1-positive fibers nerve fibers (NDI_s~1.7 *versus* 0.5 mm/mm^2, contrast Fig. 1 with Figs. 3 and 4; quantitative data in Fig. 7). These deeper, denser stromal nerve fibers were very thin, and distributed singly between collagen lamellae rather than clustered into thick trunks as in the intact cornea. This stromal nerve hyper-density appeared restricted to the ablation zone, with nerve distribution in the peripheral stroma remaining relatively normal (Figs. 4, 7). A final distinguishing feature of the healing cornea 2 weeks post-PRK was the almost complete absence of sub-basal and intra-epithelial nerves *above* the band of αSMA-positive stroma (Figs. 4, 7).

3.3.2. Four weeks after PRK (Fig. 3D, middle row of Fig. 4),—

The central epithelium appeared fully healed and the thickness of the central αSMA-positive zones had decreased. On occasion, small zones devoid of cells were observed peripheral to the ablation zone in the superficial stroma (blue zones in Fig. 4). However, the most striking observation at this timepoint was the continued absence of sub-basal and epithelial nerves above the αSMA-positive zones, while stromal nerve densities *below* the αSMA-positive zones continued to be abnormally high (Fig. 7). Peripheral nerve distribution and densities did not differ significantly from normal (Fig. 7)

3.3.3. By 12 weeks post-PRK (Fig. 3E, bottom row Fig. 4),—

Untreated corneas looked structurally normal, with no αSMA-positive zones in the stroma. Although central sub-basal nerve length returned to normal (0.73 ± 0.07mm), central NDI_e averaged only 5.6 ± 2.4 mm/mm^2, about a third normal levels, while central stromal nerves remained hyper-dense (Fig. 7). Thus, 12 weeks after PRK, nerve distribution in the central cornea remained abnormal. In contrast, nerve lengths and densities in the corneal periphery remained within the normal range (NDI_s = 0.4±0.09 mm/mm^2; NDI_e = 9.2±1.6 mm/mm^2; sub-basal length = 0.97±0.16 mm – black bars in Fig. 7).

3.4. Effects of PA on corneal nerve regeneration after PRK in the cat

3.4.1. Two weeks after PRK+ topical PA (Fig. 3F, top row Fig. 5),—

Immunohistochemical labeling showed a relatively thin αSMA-positive band in the stroma, under the epithelium. As in untreated eyes, this αSMA-positive band was almost completely devoid of corneal nerves ($NDI_{\alpha SMA}$ of 0.04 ± 0.02 mm/mm$^{2)}$, and above it, there was also an almost complete absence of sub-basal and intraepithelial nerves. Unlike untreated eyes however, the central stromal nerve density of PA-treated eyes below the αSMA-positive zone was similar to that of unoperated corneas (two-tailed t-test: $t(6)=0.98, p=0.365$). The corneal periphery outside the ablation zone also had less than a quarter of the normal NDI_e and half the NDI_e of untreated eyes post-PRK (Fig. 7). This was accompanied by an approximate halving of the length of peripheral sub-basal nerves relative to untreated eyes at

the same time-point post-PRK (Fig. 7). As such, topical PA seemed to decrease nerve densities *across the central and peripheral cornea* 2 weeks post-PRK.

3.4.2. Four weeks after PRK and 2 weeks after cessation of topical PA (Fig. 3G, middle row Fig. 5),—There was a continued, almost complete absence of sub-basal and intra-epithelial nerves in the central cornea above the ablation zone (Fig. 7), as well as inside the thick αSMA positive layer in the central stroma. However, central NDI_s was now abnormally high, while peripheral sub-basal and intra-epithelial nerve densities appeared to have recovered from their depressed levels at 2 weeks post-PRK (Fig. 7).

3.4.3. Twelve weeks post-PRK and 10 weeks after cessation of topical PA (Fig. 3H, bottom row Fig. 5),—The healed corneas looked structurally normal, with a total absence of αSMA-positive cells in the stroma. However, some small acellular zones (characterized by an absence of DAPI-positive cell nuclei, blue regions in Fig. 5) were seen on all four PA-treated corneas at this timepoint, predominantly in peripheral and mid-peripheral regions. Of note, stromal nerves did not appear to avoid such zones and were seen frequently inside them (purple nerves in Fig. 5). Sub-basal and intra-epithelial nerves also repopulated some of the central cornea above the ablation zone, but this was inconsistent (only 1/4 of the corneas had regained normal central sub-basal nerve length and none of the corneas had normal central NDI_e). Central NDI_e averaged only 3.2 ± 1.6 mm/mm^2, about a fifth normal levels – similar to the central NDI_e of untreated corneas 12 weeks post-PRK (two-tailed t-test: $t(6)=0.83, p=0.438$). In contrast with the sparse and inconsistent intra-epithelial innervation, central stromal nerve density remained high, averaging 1.3 ± 0.4 mm/mm^2. This was similar to levels seen in untreated cat corneas at this timepoint, and about 2.4 times higher than normal. Finally, while peripheral NDI_s and sub-basal nerve lengths appeared normal, peripheral NDI_e remained significantly below levels seen in untreated cat corneas (two-tailed t-test: $t(6)=4.34, p=0.0049$). Thus, 12 weeks after PRK+ topical PA, nerve distribution in the central cornea was even less normal than in untreated corneas. Moreover, peripheral intra-epithelial nerve densities were also depressed and several acellular zones developed in the peripheral stroma.

3.5. Effects of MMC on corneal nerve regeneration after PRK in the cat

3.5.1. Two weeks after PRK+ intraoperative MMC (Fig. 3I, top row Fig. 6),—Histology and immunohistochemistry revealed a remarkably well-healed cornea with the thinnest yet bands of α-SMA-positive cells in the ablation zone stroma. As in untreated eyes, nerves appeared to avoid α-SMA-positive cells, but in MMC-treated eyes, they did occasionally penetrate the central epithelium from the stroma, through gaps between the thin α-SMA-positive bands. Thus, in the present study, MMC-treated corneas were the only ones in which central sub-basal nerves were consistently observed 2 weeks post-PRK. Possibly because their length remained small (only 0.05 ± 0.1 mm over the sampled area), NDI_e remained very low, averaging 0.7 ± 0.3 mm/mm^2 (Fig. 7). The central stroma of MMC-treated eyes below the α-SMA-positive zone trended towards higher nerve densities compared to unoperated corneas, but did not reach significance (two-tailed t-test: $t(6)=2.41, p=0.053$). In the corneal periphery outside the ablation zone, all nerve distributions and densities were normal.

3.5.2. Four weeks after PRK +MMC (Fig. 3J, middle row Fig. 6),—There was a continued significant increase in central sub-basal length and intra-epithelial nerve densities above the ablation zone relative to the 2 weeks post-PRK time-point and relative to untreated corneas at the same timepoint (Fig. 7). While there were no longer any α-SMA-positive cells, they were replaced by acellular zones in the stroma, which appeared to contain nerves. Stromal nerves entered and traversed these acellular zones apparently unimpeded (purple traces in Fig. 6) and central stromal nerve density, which included these acellular zone nerves, increased to 1.6 ± 0.6 mm/mm^2, about 3x that in normal [unoperated] corneas (Fig. 7). In contrast, nerve densities in the corneal periphery remained normal (Fig. 7).

3.5.3. Twelve weeks after PRK + MMC (Fig. 3K, bottom row Fig. 6),—The healed corneas looked structurally normal, although large, co-extensive, acellular zones were now present in the anterior stroma, both in the central and peripheral cornea (blue regions in Fig. 6). Again, stromal nerves appeared completely unaffected in their trajectories by their encounter with large, cell-free zones (purple traces in Fig. 6). Moreover, large, thick nerve trunks began to re-appear in the stroma, instead of the fine, seemingly defasciculated fibers present at earlier time-points. Central NDI_s remained elevated, but both central and peripheral sub-basal nerve lengths and intra-epithelial nerve densities returned towards the normal range (Fig. 7).

4. DISCUSSION

The present study asked how decreasing fibrosis impacted corneal nerve regeneration *in vivo* during wound healing in the cat. Myopic PRK was performed over a large area and to a depth that ensured damage of intra-epithelial, sub-basal and about half the central, stromal nerves. Fibrosis was demonstrably decreased using both intra-operative MMC, a cytotoxic agent, or 2 weeks of daily, topical PA, a steroid, albeit to different degrees (MMC>>PA) and over a different time-course (MMC much faster than PA). Our results suggest that the strength of anti-fibrotic action was closely related to the success of nerve regeneration attained out to 3 months post-PRK.

4.1. Native corneal nerve regeneration after PRK

As in humans undergoing PRK, the use of a cat model in the present study induced nerve damage across a large area of cornea, and in all three corneal layers containing nerves, allowing us to make several key observations. First, in the absence of anti-fibrotic treatment, and as recently reported by our group (Jeon et al., 2018), we confirmed that regenerating corneal nerves appeared to avoid stromal regions positive for α-SMA. As a result, even a month after PRK, the central [ablation zone] cornea inside and above the α-SMA positive stroma remained devoid of nerves. We can only speculate as to the sensory consequences of this depletion; perhaps it caused absent, dulled or abnormal sensation and reflexes (Gallar et al., 2007; Hovanesian et al., 2001; Toda et al., 2001), or as reported after PRK in humans (and in contrast to laser in situ keratomileusis), sensation might be back to normal in spite of persistent abnormalities in nerve densities and morphologies (Calvillo et al., 2004; Corbett et al., 1996; Erie, 2003; Erie et al., 2005; Kauffmann et al., 1998; Linna et al., 1998; Linna and Tervo, 1997; Linna et al., 2000; Moilanen et al., 2003).

Second, even 3 months after PRK, nerve regeneration across the central ablation zone remained incomplete, with fewer-than-normal intra-epithelial nerves and too many stromal nerves. It should be noted however, that the high stromal nerve density observed might simply reflect defasciculation of nerve trunks rather than increased axonal branching in the stroma. Nonetheless, we can only guess at the functional and sensory consequences of localized abnormalities in nerve density in different corneal layers post-PRK in the cat, speculatively ranging from no effects to decreased or enhanced sensation (Bech et al., 2018; Belmonte et al., 2004b; Hovanesian et al., 2001; McCarty et al., 1996; Stein et al., 1994).

4.2. Topical steroid delays corneal nerve regeneration after PRK

As slow and incomplete as native corneal nerve regeneration was following PRK in the cat, topical application of 1% PA twice daily for 2 weeks starting immediately after the ablation appeared to further delay this process. Relevant to this, post-mortem histology showed steroid-treated eyes to have the slowest epithelial wound healing among our three treatment groups. In contrast to treatment of human patients (e.g., Nejima et al., 2005; Pérez-Santonja et al., 1999; Sauvageot et al., 2017), no bandage contact lens was used post-PRK in the cat and steroid was given both intraoperatively and then daily without waiting for epithelial healing. That early phases of epithelial wound healing were delayed in our steroid-treated cat corneas after PRK is consistent with some published results (Petroutsos et al., 1982), and may be secondary to reduced sub-epithelial hyaluronan formation (Weber et al., 2001). Poorly organized epithelia such as were seen in our steroid-treated eyes could be leaky, and this could also prolong cytokine signaling between the epithelium and the stroma (Nakamura, 2003; Wilson et al., 2001), promoting transformation of anteriorly located stromal keratocytes into α-SMA-positive myofibroblasts (Nakamura et al., 2001). However, steroids are known to suppress inflammatory chemokines in corneal myofibroblasts (Ebihara et al., 2011), which may underlie the reduced α-SMA expression (relative to untreated eyes) 2 weeks post-PRK. This reduced α-SMA expression in turn likely underlies the reduced backscatter reflectivity observed with OCT imaging at that time-point. Unfortunately, once steroid treatment stops, if the epithelium is still abnormal, stromal keratocytes could once again be exposed to cytokines from both the epithelium and the ocular surface, likely explaining the persistence of strong α-SMA staining at 4 weeks post-PRK in PA-treated eyes.

PA also appeared to have a remarkably long-lasting impact on the ability of nerves to regenerate and repopulate different corneal layers after PRK. At 2 weeks post-PRK – which also coincided with the end of topical PA treatment - the ablation zone of PA-treated eyes was devoid of sub-basal and intra-epithelial nerves. Unlike untreated eyes however, the peripheral cornea of PA-treated eyes, which presumably fell outside the ablation zone, also exhibited abnormally low intraepithelial and sub-basal nerve densities. Given the supportive role normally played by epithelial cells for corneal nerves (Araki et al., 1994; Beuerman and Schimmelpfennig, 1980; Goins, 2005; Stepp et al., 2018; Stepp et al., 2017; Ueno et al., 2012), abnormal epithelial healing may help explain why PA-treated corneas exhibited such low epithelial nerve densities. In addition, PA-treated eyes also failed to exhibit the central hyper-density of sub-ablation stromal nerve fibers seen in untreated and MMC-treated eyes at 2 weeks post-PRK. While it is possible that PA treatment preserved fasciculation in the

stroma, an alternative hypothesis is that PA inhibited axonal branch formation and neurite outgrowth. A hyper-density of stromal nerve fibers was eventually observed 4 weeks after PRK – i.e., 2 weeks after cessation of PA treatment. However, even by 12 weeks after PRK + topical PA, central epithelial and sub-basal nerves remained less dense than in untreated corneas. While the literature on this topic is relatively sparse (and non-existent with respect to trigeminal neurons), there is evidence that a single pre-treatment with Dexamethasone inhibits neurite outgrowth in cultured PC12 cells treated with nerve growth factor, and that it does so by blocking phosphorylation of Akt and ERK1/2 in a glucocorticoid receptor-dependent manner (Terada et al., 2014). Whether relevant receptors are present on trigeminal axons in the cornea, and what intracellular signaling pathways may be activated by PA remain to be determined. Steroids are also known to inhibit immune cell function (Kupferman and Leibowitz, 1975) and since some of the immune cells which invade the cornea during wound healing release cytokines that are known to promote nerve regeneration (Liu et al., 2012; Müller et al., 2003), this may have contributed to the inhibitory effects of steroids on corneal nerve densities. Finally, we should note that a reduction in corneal epithelial innervation was recently described in a study following daily application of 1% PA for 2 weeks in otherwise untouched (i.e. undamaged) wild-type mice (Chen et al., 2017), suggesting perhaps that PA can cause retraction of intact nerve endings in the epithelium.

4.3. Intra-operative MMC enhances corneal nerve regeneration after PRK

That MMC seemed to improve epithelial wound healing in the present experiments differs from results of one previous clinical study (Kremer et al., 2012). However, that study used other agents simultaneously with MMC, including topical steroid, topical non-steroidal anti-inflammatory drops, bandage contact lenses, and benzalkonium chloride within administered drops – all of which are known to negatively impact epithelial wound healing. More consistent with our results, Pal-Ghosh, Stepp and colleagues showed a stabilizing effect of MMC on the damaged corneal epithelium, as well as changes in epithelial gene expression and preservation of L1CAM on nerves that together, may underlie enhanced sub-basal nerve regeneration in their mouse model (Pal-Ghosh et al., 2016; Stepp et al., 2018). However, we posit that part of the facile epithelial and sub-basal nerve regeneration seen in the ablation zone of our MMC-treated cat eyes was also due to the fact that those eyes experienced minimal myofibroblast transformation, as indicated by briefer and reduced α-SMA staining post-PRK. MMC is known to impact keratocytes, decreasing their ability to multiply and differentiate into myofibroblasts. Confocal examination of human myopes after PRK showed reduced keratocyte activation, decreased stromal cell density and reduced repopulation of the anterior stroma in MMC-treated eyes (Gambato et al., 2005). MMC induces DNA intra-strand crosslinking, which is thought to inhibit replication, alter gene transcription, and cause cell death (Tomasz, 1995). In addition, MMC may cause DNA damage in surviving corneal keratocytes, impacting long-term behavior, including the ability to undergo pro-fibrotic transformation (Jester et al., 2012). Interestingly, nerves did not avoid the large acellular zones that developed in the sub-ablation and peripheral stroma of MMC-treated cat eyes. Thus, keratocytes (or other cell types) were not needed to “attract” re-growing nerves into particular regions of the stroma after PRK.

4.4. CONCLUSIONS

While important for restoring the structural integrity of the cornea during wound healing, fibrosis has the unfortunate side-effect of reducing clarity and altering corneal refractive properties (Bühren et al., 2009; Lohmann et al., 1991; Nagy et al., 2007; Siganos et al., 1999). Recent work suggests that it may also negatively impact neurite outgrowth (Jeon et al., 2018), prompting the present study, which asked if MMC and PA, two commonly-used antifibrotics, might improve nerve regeneration post-PRK. Intra-operative application of 0.02% MMC decreased α-SMA staining and was associated with faster restoration of corneal innervation than no treatment. In contrast, intra-operative, then twice daily application of 1% PA for 2 weeks, which generated longer-lasting α-SMA staining, delayed restoration of central innervation and decreased peripheral intra-epithelial nerve densities. The mechanisms underlying the effects of PA and MMC on nerves remain to be determined, as does the relationship between post-operative changes in nerve distribution and sensation. Finally, much current research aims to find better anti-fibrotics for the cornea. In this context, the present work highlights the importance of evaluating how these agents affect damaged and regenerating corneal nerves as a key factor in establishing their safety and efficacy.

ACKNOWLEDGEMENTS AND FUNDING

Research reported in this publication was supported by the National Eye Institute of the National Institutes of Health (R01 EY015836 and Core Grant P30 EY001319 to the Center for Visual Science) and an unrestricted grant to the University of Rochester's Department of Ophthalmology from the Research to Prevent Blindness Foundation (RPB). The content of this article is solely the responsibility of the authors and does not necessarily represent the official views of our granting agencies.

Financial Support:

This work was supported by the National Eye Institute of the National Institutes of Health (R01 EY015836 and Core Grant P30 EY001319 to the Center for Visual Science), and in part by an Unrestricted Grant to the Department of Ophthalmology from Research to Prevent Blindness, USA.

Abbreviations

ANOVA	analysis of variance
α-SMA	alpha smooth muscle actin
DAPI	4′,6-diamidino-2-phenylindol
H&E	Hematoxylin and Eosin
HSV-1	herpes simplex virus 1
IgG	Immunoglobulin G
MMC	Mitomycin C
NDI	nerve density index
OCT	optical coherence tomography
PA	prednisolone acetate

PBS	phosphate buffered saline
PRK	photorefractive keratectomy
Tuj-1	antibody against beta III-tubulin

REFERENCES

Araki K, Ohashi Y, Kinoshita S, Hayashi K, Kuwayama Y, Tano Y, 1994 Epithelial wound healing in the denervated cornea. Current Eye Research 13, 203–211. [PubMed: 8194368]

Bahn CF, Meyer RF, MacCallum DK, Lillie JH, Lovett EJ, Sugar A, Martonyi CL, 1982 Penetrating keratoplasty in the cat. A clinically-applicable model. Ophthalmology 89, 687–699. [PubMed: 6750492]

Bech F, Gonzalez-Gonzalez O, Artime E, Serrano J, Alcalde I, Gallar J, Merayo-Lloves J, Belmonte C, 2018 Functional and morphologic alterations in mechanical, polymodal, and cold sensory nerve fibers of the cornea following photorefractive keratectomy. Investigative Ophthalmolgy and Visual Science 59, 2281–2292.

Belmonte C, Acosta MC, Gallar J, 2004a Neural basis of sensation in intact and injured corneas. Experimental Eye Research 78, 513–525. [PubMed: 15106930]

Belmonte C, Acosta MC, Gallar J, 2004b Neural basis of sensation in intact and injured corneas. Exp Eye Res 78, 513–525. [PubMed: 15106930]

Belmonte C, Garcia-Hirschfeld J, Gallar J, 1997 Neurobiology of ocular pain. Progress in Retinal and Eye Research 16, 117–156.

Beuerman RW, Schimmelpfennig B, 1980 Sensory denervation of the rabbit cornea affects epithelial properties. Experimental Neurology 69, 196–201. [PubMed: 7389846]

Bühren J, Nagy LJ, Swanton JN, Kenner S, MacRae S, Phipps RP, Huxlin KR, 2009 Optical effects of anti-TGF[beta] treatment after photorefractive keratectomy in a cat model. Investigative Ophthalmology and Visual Science 50, 634–643. [PubMed: 18952913]

Bühren J, Yoon G, Kenner S, Artrip S, MacRae S, Huxlin KR, 2007a The effect of pupil decentration on lower- and higher-order aberrations after myopic photorefractive keratectomy (PRK) in a cat model, ARVO, Ft. Lauderdale.

Bühren J, Yoon G, Kenner S, MacRae S, Huxlin KR, 2007b The effect of optical zone decentration on lower- and higher-order aberrations after photorefractive keratectomy in a cat model. Investigative Ophthalmology and Vision Science 48, 5806–5814.

Bühren J, Yoon G, MacRae S, Huxlin KR, 2010 Contribution of optical zone decentration and pupil dilation on the change of optical quality after myopic photorefractive keratectomy in a cat model. Journal of Refractive Surgery 26, 183–190. [PubMed: 20229950]

Calvillo MP, McLaren JW, Hodge DO, Bourne WM, 2004 Corneal reinnervation after LASIK: prospective 3-year longitudinal study. Investigative Ophthalmolgy and Visual Science 45, 3991–3996.

Carones F, Brancato R, Venturi E, Scialdone A, Bertuzzi A, Tavola A, 1993 Efficacy of corticosteroids in reversing regression after myopic photorefractive keratectomy. Refractive and Corneal Surgery 9, S52–56. [PubMed: 8499380]

Chan-Ling T, 1989 Sensitivity and neural organization of the cat cornea. Investigate Ophthalmolgy and Visual Science 30, 1075–1082.

Chen FY, Lee A, Ge S, Nathan S, Knox SM, McNamara NA, 2017 Aire-deficient mice provide a model of corneal and lacrimal gland neuropathy in Sjögren's syndrome. PLoS One 12, e0184916. [PubMed: 28926640]

Corbett MC, Prydal JI, Verma S, Oliver KM, Pande M, Marhsall J, 1996 An in vivo investigation of the structures responsible for corneal haze after photorefractive keratectomy and their effect on visual function. Ophthalmology 103, 1366–1380. [PubMed: 8841294]

Ebihara N, Ohtomo K, Tokura T, Ushio H, Murakami A, 2011 Effect of tacrolimus on chemokine production by corneal myofibroblasts via toll-like receptors, compared with cyclosporine and dexamethasone. Cornea 30, 702–708. [PubMed: 21282993]

Erie JC, 2003 Corneal wound healing after photorefractive keratectomy. Transactions of the American Ophthalmological Society 101, 294–333.

Erie JC, McLaren JW, Hodge DO, Bourne WM, 2005 Recovery of corneal sub-basal nerve density after PRK and LASIK. American Journal of Ophthalmology 140, 1059–1064. [PubMed: 16376651]

Esquenazi S, He J, Bazan NG, Bazan HEP, 2005 Comparison of corneal wound healing response in photorefractive keratectomy and laser-assisted subepithelial keratectomy. Journal of Cataract & Refractive Surgery 31, 1632–1639.

Fagerholm P, Hamberg-Nystrom H, Tengroth B, Epstein D, 1994 Effect of postoperative steroids on the refractive outcome of photorefractive keratectomy for myopia with the summit excimer laser. Journal of Cataract & Refractive Surgery 20, 212–215.

Gallar J, Acosta MC, Gutierrez AR, Belmonte C, 2007 Impulse activity in corneal sensory nerve fibers after photorefractive keratectomy. Investigative ophthalmology & visual science 48, 4033–4037. [PubMed: 17724184]

Gambato C, Ghirlando A, Moretto E, Busato F, Midena E, 2005 Mitomycin C modulation of corneal wound healing after photorefractive keratectomy in highly myopic eyes. Ophthalmology 112, 208–218; [PubMed: 15691552]

Gartry DS, Kerr Muir M, Marshall J, 1993 The effect of topical corticosteroids on refraction and corneal haze following excimer laser treatment of myopia: an update. A prospective, randomised, double-masked study. Eye 7 (Pt 4), 584–590. [PubMed: 8253244]

Goins K, 2005 New insights into the diagnosis and treatment of neurotrophic keratopathy. Ocular Surface 3, 96–110. [PubMed: 17131013]

Guaiquil VH, Pan Z, Karagianni N, Fukuoka S, Alegre G, Rosenblatt MI, 2014 VEGF-B selectively regenerates injured peripheral neurons and restores sensory and trophic functions. Proceedings of the National Academy of Science of the United State of America 111, 17272–17277.

Guthoff RF, Wienss H, Hahnel C, Wree A, 2005 Epithelial innervation of human cornea: a three-dimensional study using confocal laser scanning fluorescence microscopy. Cornea 24, 608–613. [PubMed: 15968170]

Harris DL, Yamaguchi T, Hamrah P, 2018 A Novel Murine Model of Radiation Keratopathy. Investigative Ophthalmolgy and Visual Science 59, 3889–3896.

Hovanesian JA, Shah SS, Maloney RK, 2001 Symptoms of dry eye and recurrent erosion syndrome after refractive surgery. J Cataract Refract Surg 27, 577–584. [PubMed: 11311627]

Hughes A, 1977 The topography of vision in mammals of contrasting life style: comparative optics and retinal organization, Handbook of Sensory Physiology, V.II/5. Springer Verlag, Berlin.

Huxlin KR, Hindman HB, Jeon K-I, Bühren J, MacRae S, DeMagistris M, Ciufo D, Sime PJ, Phipps RP, 2013 Topical Rosiglitazone is an effective anti-scarring agent in the cornea. PLoS One 8, e70785. [PubMed: 23940641]

Jeon K-I, Hindman HB, Bubel T, McDaniel T, DeMagistris M, Callan C, Huxlin KR, 2018 Corneal myofibroblasts inhibit regenerating nerves during wound healing. Scientific Reports, in press,

Jeon K-I, Kulkarni A, Woeller CF, Phipps RP, Sime PJ, Hindman HB, Huxlin KR, 2014 Inhibitory effects of PPARγ ligands on TGFβ1-induced corneal myofibroblast transformation. The American Journal of Pathology 184, 1429–1445. [PubMed: 24650561]

Jester JV, Huang J, Fisher S, Spiekerman J, Chang JH, Wright WE, Shay JW, 2003 Myofibroblast differentiation of normal human keratocytes and hTERT, extended-life human corneal fibroblasts. Investigative Ophthalmology and Vision Science 44, 1850–1858.

Jester JV, Nien CJ, Vasiliou V, Brown DJ, 2012 Quiescent keratocytes fail to repair MMC induced DNA damage leading to the long-term inhibition of myofibroblast differentiation and wound healing. Molecular Vision 18, 1828–1839. [PubMed: 22815636]

Jester JV, Petroll WM, Cavanagh HD, 1999 Corneal stromal wound healing in refractive surgery: the role of myofibroblasts. Progress in Retinal & Eye Research 18, 311–356.

Jester JV, Petroll WM, Feng W, Essepian J, Cavanagh HD, 1992 Radial keratotomy. I. The wound healing process and measurement of incisional gape in two animal models using in vivo confocal microscopy. Investigate Ophthalmolgy and Visual Science 33, 3255–3270.

Kauffmann T, Bodanowitz S, Hesse L, Kroll P, 1998.

Kim TI, Pak JH, Lee SY, Tchah H, 2004 Mitomycin C-induced reduction of keratocytes and fibroblasts after photorefractive keratectomy. Investigative Ophthalmolgy and Visual Science 45, 2978–2984.

Kremer I, Ehrenberg M, Levinger S, 2012 Delayed epithelial healing following photorefractive keratectomy with mitomycin C treatment. Acta Ophthalmologica 90, 271–276. [PubMed: 20456254]

Kupferman A, Leibowitz HM, 1975 Anti-inflammatory effectiveness of topically administered corticosteroids in the cornea without epithelium. Investigative Ophthalmolgy and Visual Science 14, 252–255.

Labbe A, Liang Q, Wang Z, Zhang Y, Xu L, Baudouin C, Sun X, 2013 Corneal nerve structure and function in patients with non-Shögren dry eye: clinical correlations. Investigative Ophthalmolgy and Visual Science 54, 5144–5150.

Lambiase A, Sacchetti M, Bonini S, 2012 Nerve growth factor therapy for corneal disease. Current Opinion in Ophthalmology 23, 296–302. [PubMed: 22543481]

Linna TU, Perez-Santonja JJ, Tervo KM, Sakla HF, Sanz JL, Tervo TM, 1998 Recovery of corneal nerve morphology following laser in situ keratomileusis. Experimental Eye Research 66, 755–763. [PubMed: 9657908]

Linna TU, Tervo T, 1997 Real-time confocal microscopic observations on human corneal nerves and wound healing after excimer laser photorefractive keratectomy. Current Eye Research 16, 640–649. [PubMed: 9222080]

Linna TU, Vesaluoma MH, Perez-Santonja JJ, Petroll WM, Alio JL, Tervo TM, 2000 Effect of myopic LASIK on corneal sensitivity and morphology of sub-basal nerves. Investigative Ophthalmology and Visual Science 41, 393–397. [PubMed: 10670467]

Liu Q, Smith CW, Zhang W, Burns AR, Li Z, 2012 NK Cells Modulate the Inflammatory Response to Corneal Epithelial Abrasion and Thereby Support Wound Healing. The American Journal of Pathology 181, 452–462. [PubMed: 22728064]

Lohmann CP, Gartry DS, Muir MK, Timberlake GT, Fitzke FW, Marshall J, 1991 Corneal haze after excimer laser refractive surgery: objective measurements and functional implications. Eur J Ophthalmol 1, 173–180. [PubMed: 1821211]

Machat JJ, 1993 Double-blind corticosteroid trial in identical twins following photorefractive keratectomy. Refractive and Corneal Surgery 9, S105–107. [PubMed: 8499355]

Majmudar PA, Forstot SL, Dennis RF, Nirankari VS, Damiano RE, Brenart R, Epstein RJ, 2000 Topical mitomycin-C for subepithelial fibrosis after refractive corneal surgery. Ophthalmology 107, 89–94. [PubMed: 10647725]

Marfurt CF, Cox J, Deek S, Dvorscak L, 2010a Anatomy of the human corneal innervation. Exp Eye Res 90, 478–492. [PubMed: 20036654]

Marfurt CF, Cox J, Deek S, Dvorscak L, 2010b Anatomy of the human corneal innervation. Experimental Eye Research 90, 478–492. [PubMed: 20036654]

McCarty CA, Garrett SK, Aldred GF, Taylor HR, 1996 Assessment of subjective pain following photorefractive keratectomy. Melbourne Excimer Laser Group. J Refract Surg 12, 365–369. [PubMed: 8705712]

Miller M, Cho JY, McElwain K, McElwain S, Shim JY, Manni M, Baek JS, Broide DH, 2006 Corticosteroids prevent myofibroblast accumulation and airway remodeling in mice. American Journal of Physiology - Lung Cellular and Molecular Physiology 290, L162–169. [PubMed: 16344333]

Moilanen JAO, Vesaluoma MH, Müller LJ, Tervo TM, 2003 Long-term corneal morphology after PRK by in vivo confocal microscopy. Investigative Ophthalmolgy and Visual Science 44, 1064–1069.

Moreira M, Fagundes DJ, de Jesus Simoes M, Taha MO, Perez LM, Bazotte RB, 2010 The effect of liposome-delivered prednisolone on collagen density, myofibroblasts, and fibrous capsule thickness around silicone breast implants in rats. Wound Repair and Regeneration 18, 417–425. [PubMed: 20636553]

Muller LJ, Marfurt CF, Kruse F, Tervo TM, 2003 Corneal nerves: structure, contents and function. Exp Eye Res 76, 521–542. [PubMed: 12697417]

Müller LJ, Marfurt CF, Kruse F, Tervo TMT, 2003 Corneal nerves: structure, contents and function. Experimental Eye Research 76, 521–542. [PubMed: 12697417]

Murata Y, Masuko S, 2006 Peripheral and central distribution of TRPV1, substance P and CGRP of rat corneal neurons. Brain Research 1085, 87–94. [PubMed: 16564032]

Nagy LJ, MacRae S, Yoon G, Cox I, Huxlin KR, 2007 Photorefractive keratectomy in the cat eye: biological and optical outcomes. Journal of Cataract and Refractive Surgery 33, 1051–1064. [PubMed: 17531702]

Nakamura K, 2003 Interaction between injured corneal epithelial cells and stromal cells. Cornea 22, S35–S47. [PubMed: 14703706]

Nakamura K, Kurosaka D, Bissen-Miyajima H, Tsubota K, 2001 Intact corneal epithelium is essential for the prevention of stromal haze after laser assisted in situ keratomileusis. Br J Ophthalmol 85, 209–213. [PubMed: 11159488]

Nejima R, Miyata K, Tanabe T, Okamoto F, Hiraoka T, Kiuchi T, Oshika T, 2005 Corneal barrier function, tear film stability, and corneal sensation after photorefractive keratectomy and laser in situ keratomileusis. American Journal of Ophthalmology 139, 64–71. [PubMed: 15652829]

Netto MV, Mohan RR, Ambrosio R, Jr., Hutcheon AE, Zieske JD, Wilson SE, 2005 Wound healing in the cornea: a review of refractive surgery complications and new prospects for therapy. Cornea 24, 509–522. [PubMed: 15968154]

Netto MV, Mohan RR, Sinha S, Sharma A, Dupps WJ, Jr., Wilson SE, 2006a Stromal haze, myofibroblasts and surface irregularity after PRK. Experimental Eye Research 82, 788–797. [PubMed: 16303127]

Netto MV, Mohan RR, Sinha S, Sharma A, Gupta PC, Wilson SE, 2006b Effect of prophylactic and therapeutic mitomycin C on corneal apoptosis, cellular proliferation, haze, and long-term keratocyte density in rabbits. J Refract Surg 22, 562–574. [PubMed: 16805119]

Ozaki K, Terayama Y, Matsuura T, 2018 Extended Duration of Hyperglycemia Result in Human-Like Corneal Nerve Lesions in Mice With Alloxan- and Streptozotocin-Induced Type 1 Diabetes. Investigative Ophthalmolgy and Visual Science 59, 5868–5875.

Pal-Ghosh S, Pajoohesh-Ganji A, Tadvalkar G, Kyne BM, Guo X, Zieske JD, Stepp MA, 2016 Topical Mitomycin-C enhances subbasal nerve regeneration and reduces erosion frequency in the debridement wounded mouse cornea. Experimental Eye Research 146, 361–369. [PubMed: 26332224]

Pérez-Santonja JJ, Sakla HF, Cardona C, Chipont E, Alió JL, 1999 Corneal sensitivity after photorefractive keratectomy and laser in situ keratomileusis for low myopia. American Journal of Ophthalmology 127, 497–504. [PubMed: 10334340]

Petroutsos G, Guimaraes R, Giraud JP, Pouliquen Y, 1982 Corticosteroids and corneal epithelial wound healing. Br J Ophthalmol 66, 705–708. [PubMed: 6896993]

Radhakrishnan S, Rollins AM, Roth JE, Yazdanfar S, Westphal V, Bardenstein DS, Izatt JA, 2001 Real-time optical coherence tomography of the anterior segment at 1310 nm. Archives of Ophthalmology 119, 1179–1185. [PubMed: 11483086]

Salomao MQ, Wison SE, 2009 Corneal molecular and cellular biology update for the refractive surgeon. Journal of Refractive Surgery 25, 459–466. [PubMed: 19507799]

Santhiago MR, Netto MV, Wilson SE, 2012 Mitomycin C: Biological Effects and Use in Refractive Surgery. Cornea 31, 311–321. [PubMed: 22157595]

Sarkar J, Chaudhary S, Jassim SH, Ozturk O, Chamon W, Ganesh B, Tibrewal S, Gandhi S, Byun Y-S, Hallak J, Mahmud DL, Mahmud N, Rondelli D, Jain S, 2013 CD11b+GR1+ myeloid cells secrete NGF and promote trigeminal ganglion neurite growth: implications for corneal nerve regeneration Investigative Ophthalmolgy and Visual Science 54, 5920–5936.

Sauvageot P, Julio G, de Toledo JA, Charoenrook V, Barraquer RI, 2017 Femtosecond laser-assisted laser in situ keratomileusis versus photorefractive keratectomy: effect on ocular surface condition. Journal of Cataract and Refractive Surgery 43, 167–173. [PubMed: 28366362]

Schipper I, Suppelt C, Gebbers JO, 1997 Mitomycin C reduces scar formation after excimer laser (193 nm) photorefractive keratectomy in rabbits. Eye 11 (Pt 5), 649–655. [PubMed: 9474312]

Seyed-Razavi Y, Chinnery HR, McMenamin PG, 2014 A novel association between resident tissue macrophages and nerves in the peripheral stroma of the murine cornea. Investigative Ophthalmolgy and Visual Science 55, 1313–1320.

Shaheen BS, Bakir M, Jain S, 2014 Corneal nerves in health and disease. Survey of Ophthalmology 59, 263–285. [PubMed: 24461367]

Shoji T, Nakanishi I, Suzuki A, Hayashi T, Togawa M, Okada N, Imai E, Hori M, Tsubakihara Y, 2000 Early treatment with corticosteroids ameliorates proteinuria, proliferative lesions, and mesangial phenotypic modulation in adult diffuse proliferative IgA nephropathy. Am J Kidney Dis 35, 194–201. [PubMed: 10676716]

Siganos DS, Katsanevaki VJ, Pallikaris IG, 1999 Correlation of subepithelial haze and refractive regression 1 month after photorefractive keratectomy for myopia. Journal of Refractive Surgery 15, 338–342. [PubMed: 10367577]

Stein R, Stein HA, Cheskes A, Symons S, 1994 Photorefractive keratectomy and postoperative pain. Am J Ophthalmol 117, 403–405. [PubMed: 8129020]

Stepp MA, Pal-Ghosh S, Tadvalkar G, Li L, Brooks SR, Morasso MI, 2018 Molecular basis of Mitomycin C enhanced corneal sensory nerve repair after debridement wounding. Scientific Reports 8, 1–13. [PubMed: 29311619]

Stepp MA, Tadvalkar G, Hakh R, Pal-Ghosh S, 2017 Corneal Epithelial Cells Function as Surrogate Schwann Cells for Their Sensory Nerves. Glia 65, 851–863. [PubMed: 27878997]

Terada K, Kojima Y, Watanabe T, Izumo N, Chiba K, Karube Y, 2014 Inhibition of nerve growth factor-induced neurite outgrowth from PC12 cells by Dexamethasone: signaling pathways through the glucocorticoid receptor and phosphorylated Akt and ERK1/2. PLoS One 9, e93223 [PubMed: 24667984]

Toda I, Asano-Kato N, Komai-Hori Y, Tsubota K, 2001 Dry eye after laser in situ keratomileusis. Am J Ophthalmol 132, 1–7. [PubMed: 11438046]

Tomasz M, 1995 Mitomycin c: Small, fast and deadly (but very selective). Chemical Biology 2, 575–579.

Ueno H, Ferrari G, Hattori T, Saban DR, Katikireddy KR, Chauhan SK, Dana R, 2012 Dependence of corneal stem/progenitor cells on ocular surface innervation. Investigative Ophthalmolgy and Visual Science 53, 867–872.

Vigo L, Scandola E, Carones F, 2003 Scraping and Mitomycin C to treat haze and regression after photorefractive keratectomy for myopia. Journal of Refractive Surgery 19, 449–454. [PubMed: 12899477]

Wang J, Simpson TL, Fonn D, 2004 Objective measurements of corneal light-backscatter during corneal swelling, by optical coherence tomography. Investigative Ophthalmology and Visual Science 45, 3493–3498. [PubMed: 15452054]

Weber BA, Gan L, Fagerholm PP, 2001 Short-term impact of corticosteroids on hyaluronan and epithelial hyperplasia in the rabbit cornea after photorefractive keratectomy. Cornea 20, 321–324. [PubMed: 11322424]

Wilson SE, 2002 Analysis of the keratocyte apoptosis, keratocyte proliferation and myofibroblast transformation responses after photorefractive keratectomy and laser in situ keratomileusis. Transactions of the American Ophthalmological Society 100, 411–433. [PubMed: 12545703]

Wilson SE, Mohan RR, Mohan RR, Ambrosio R, Hong JW, Lee JS, 2001 The corneal wound healing response: cytokine-mediated interaction of the epithelium, stroma and inflammatory cells. Progress in Retinal and Eye Research 20, 625–637. [PubMed: 11470453]

Yam GH, Williams GP, Setiawan M, Yusoff NZ, Lee XW, Htoon HM, Zhou L, Fuest M, Mehta JS, 2017 Nerve regeneration by human corneal stromal keratocytes and stromal fibroblasts. Sci Rep 7, 45396. [PubMed: 28349952]

Yamada N, Matsuda R, Morishige N, 2008 Open clinical study of eye-drops containing tetrapeptides derived from substance P and insulin-like growth factor-1 for treatment of persistent corneal epithelial defects associated with neurotrophic keratopathy. British Journal of Ophthalmology 92, 896–900. [PubMed: 18511539]

Zhang M, Zhou Q, Luo Y, Nguyen T, Rosenblatt MI, Guaiquil VH, 2018 Semaphorin3A induces nerve regeneration in the adult cornea - a switch from its repulsive role in development. Plos One 13(1), 1–16.

Highlights

- Myofibroblasts inhibit neurite outgrowth in vitro
- Topical steroids and mitomycin-C decrease myofibroblasts differentiation to different extents
- Decreasing myofibroblast differentiation in vivo speeds up cornea nerve regeneration after PRK
- Topical antifibrotics should be careful evaluated for their effects on corneal nerves

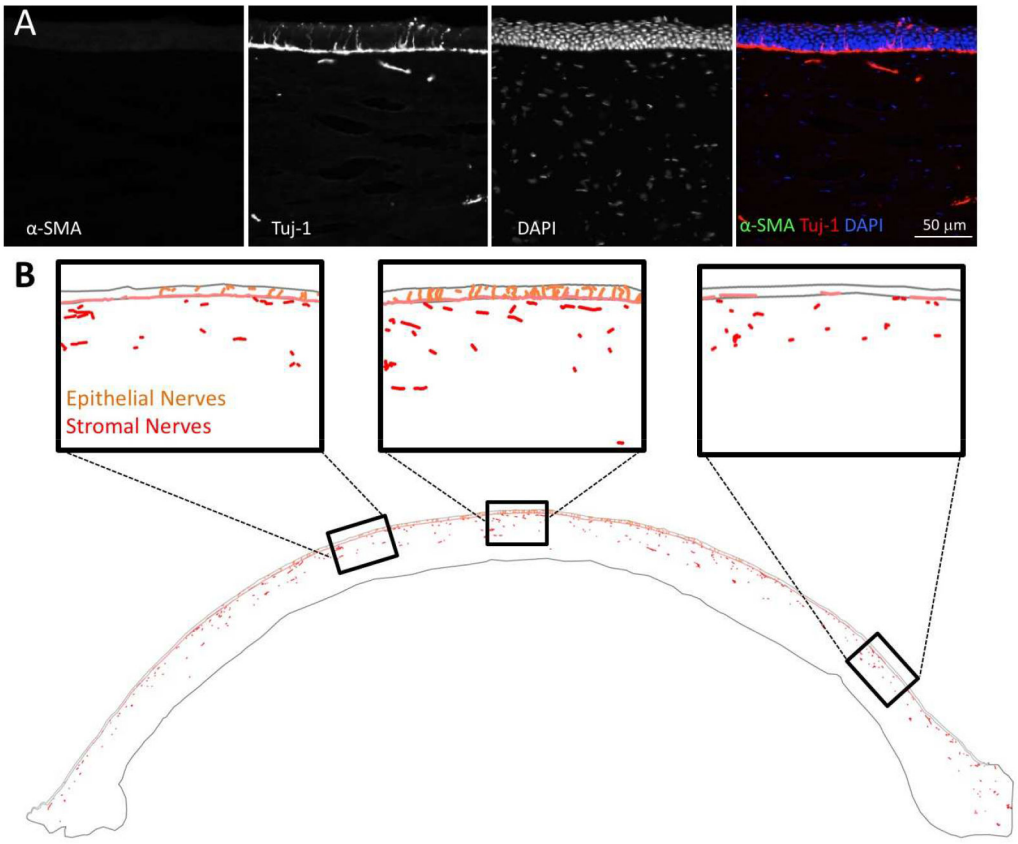

Figure 1. Immunohistochemical staining and analysis of feline corneas.

A. Monochrome photographs of triple-stained, intact, central, feline corneas showing expression of (from left to right) α-SMA, Tuj-1, and DAPI. The last image is a composite of the first three. Note sparse, thick cords of Tuj-1 positive corneal nerves in the anterior stroma, the almost continuous sub-basal nerves right under the epithelium and the thin nerve endings visible between epithelial cells. **B.** Tracing of an entire cat corneal cross section (unoperated) performed in Neurolucida, and illustrating with differential color-coding, the different layers in which corneal nerve densities were analyzed. Insets show higher power views of the central, mid-peripheral and peripheral regions of the cornea.

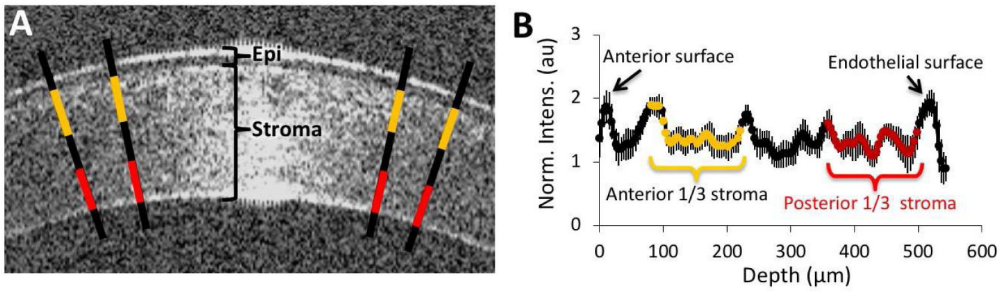

Figure 2: OCT imaging methods and analysis.

A. Magnified OCT image of the central cornea of a cat in the present study. Backscatter reflectivity was estimated over 4 lines drawn perpendicular to the cornea's surface as detailed in the text. Yellow and red segments on each line denote the approximate extent of the anterior and posterior stromal segments (respectively) over which intensity was computed in each image. Epi=epithelium. **B**. Sample reflectivity profile generated across 4 lines from the epithelium to the endothelium. Values represent the mean and standard deviation of the relative pixel intensity at each location across the cornea's depth. Yellow and red data points indicate the approximate location of the anterior and posterior thirds of the cornea.

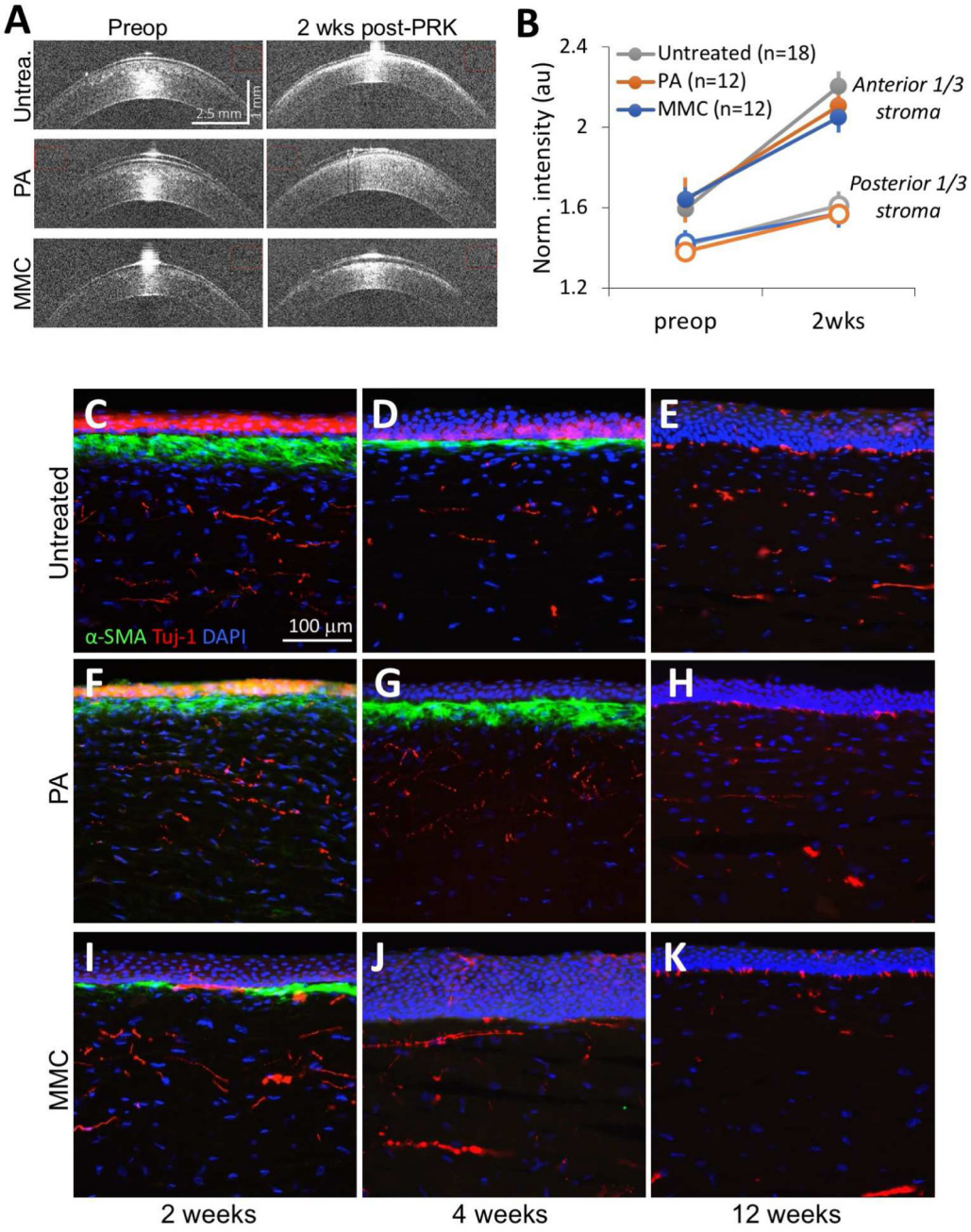

Figure 3. Fibrosis post-PRK: effect of post-operative treatments.

A. OCT images taken preoperatively and 2 weeks after PRK in a cat eye from each treatment group. Note the markedly increased anterior stromal reflectivity in the post-operative eyes, which appears less intense but more extensive in depth for the PA-treated eye (which also appears swollen), and thinner in the MMC-treated eye. **B.** Plot of normalized backscatter intensity pre-operatively and 2 weeks after PRK in the anterior and posterior thirds of the cornea of all cats and treatment groups examined. Intensity increased in all eyes post-operatively, but did so dramatically more in the anterior than the posterior cornea. Note also that untreated corneas exhibited a greater increase in reflectivity than either the PA or

MMC-treated eyes at 2 weeks post-PRK (see text for statistics). **C-K.** Immunohistochemical staining of feline corneas at different times post-PRK showing expression of α-SMA (green), Tuj-1 (red), and DAPI (blue). Scale bar = 100 μm for all photos.

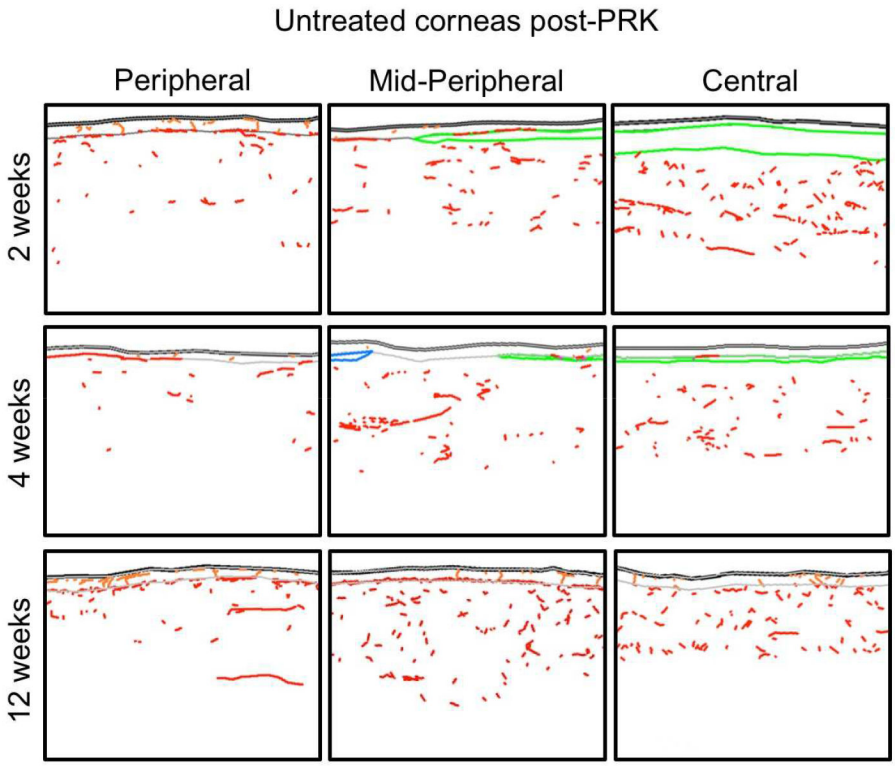

Figure 4. Sample tracings of immuno-stained corneal sections from the untreated group at different times post-PRK.

The 3 columns show illustrative tracings from the peripheral, mid-peripheral and central corneas of 3 different cat eyes. Red and orange: Tuj-1 positive corneal nerves in stroma and epithelial layers, respectively. Green: regions positive for α-SMA. In all cases, the epithelium is shown at the top of each image.

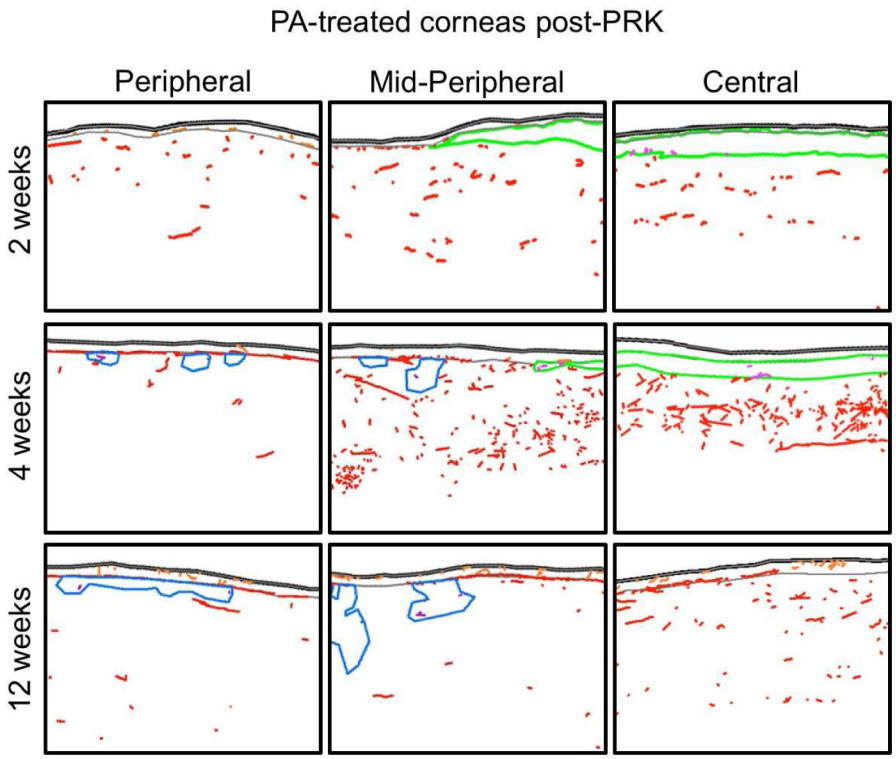

Figure 5. Sample tracings of immuno-stained corneal sections from the PA-treated group at different times post-PRK.

The 3 columns show illustrative tracings from the peripheral, mid-peripheral and central corneas of 3 different cat eyes. Red, orange and purple nerves: Tuj-1 positive corneal nerves in stroma, epithelium and acellular zones, respectively. Green: regions positive for α-SMA. Blue: acellular zones. In all cases, the epithelium is shown at the top of each image.

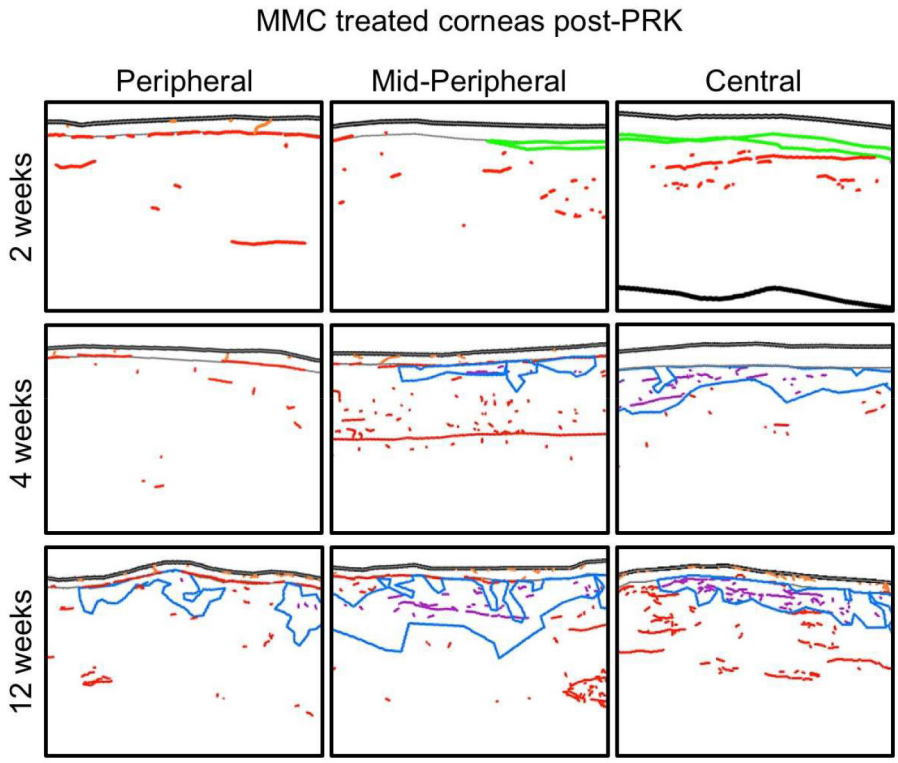

Figure 6. Sample tracings of immuno-stained corneal sections from the MMC-treated group at different times post-PRK.

The 3 columns show illustrative tracings from the peripheral, mid-peripheral and central corneas of 3 different cat eyes. Red, orange and purple nerves: Tuj-1 positive corneal nerves in stroma, epithelium and acellular zones, respectively. Blue: acellular zones. In all cases, the epithelium is shown at the top of each image.

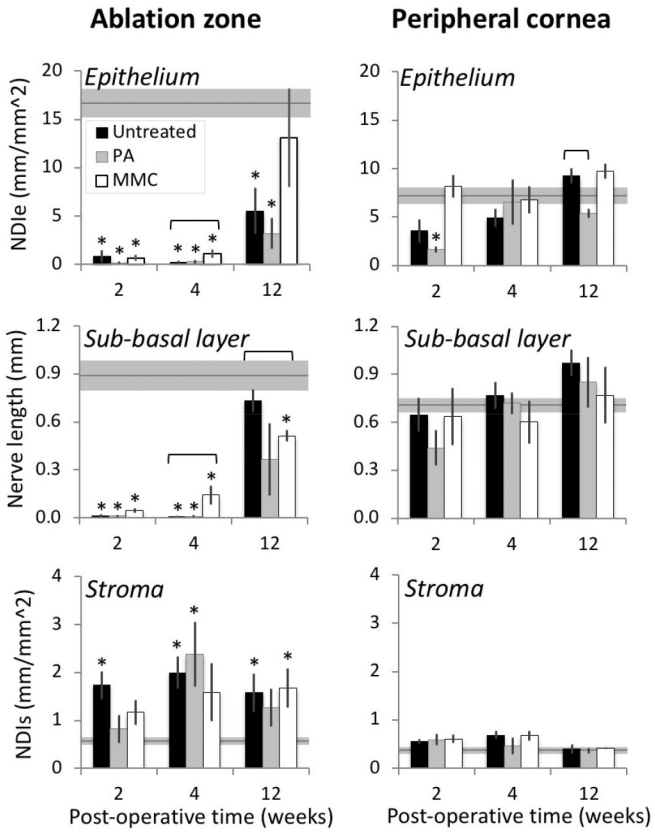

Figure 7. Quantitative analysis of nerve distributions in central ablation zone and peripheral cat corneas post-PRK.

Grey lines and shaded box indicate mean ± standard error of the mean (SEM) of values obtained in normal, unoperated control corneas (n=4). NDIe: nerve density index in the epithelium. NDIs: nerve density index in the stroma. All data points are means ± SEM. * indicates statistically significant difference relative to control (unoperated) corneas at $p<0.05$ level, computed using two-tailed Student's t-tests. Horizontal brackets over columns indicated statistically significant differences relative to untreated corneas (black bars) at $p<0.05$ level, computed using two-tailed Student's t-tests. See text for additional descriptive statistics.

Table 1.

Number of eyes and cats that underwent photorefractive keratectomy (PRK), followed either by no treatment, topical Prednisolone Acetate (PA) or Mitomycin C (MMC). Number of eyes processed for histological analysis at each of the different post-operative time-points are shown.

		Untreated	PA	MMC
# eyes (#cats) undergoing PRK		16 (8)	12 (6)	12(6)
# eyes (# cats) sampled for histology	2 weeks	6 (3)	4 (2)	4(2)
	4 weeks	6 (3)	4 (2)	4(2)
	12 weeks	4 (2)	4 (2)	4(2)